Fabrication and Characterization of Recombinant Silk#Elastin#Like#Protein (SELP) Fiber

HHS Public Access

Author manuscript

Macromol Biosci. Author manuscript; available in PMC 2020 January 15.

Published in final edited form as:

Macromol Biosci. 2018 December ; 18(12): e1800265. doi:10.1002/mabi.201800265.

Fabrication and characterization of recombinant Silk-Elastin-Like-Protein (SELP) fiber

Erin G. Roberts[1,†], **Nae-Gyune Rim**[2,†], **Wenwen Huang**[3,†], **Anna Tarakanova**[4], **Jingjie Yeo**[3,4,5], **Markus J. Buehler**[4], **David L. Kaplan**[3], **Joyce Y. Wong**[1,2,*]

[1]Division of Materials Science and Engineering, Boston University, Boston, Massachusetts 02215, USA

[2]Department of Biomedical Engineering, Boston University, Boston, Massachusetts 02215, USA

[3]Department of Biomedical Engineering, Tufts University, Medford, Massachusetts 02155, USA

[4]Department of Civil and Environmental Engineering, Massachusetts Institute of Technology, Cambridge, Massachusetts 02139, USA

[5]Institute of High Performance Computing, A*STAR, 1 Fusionopolis Way, Singapore 138632, Singapore

Abstract

Silk–elastin-like protein polymers (SELPs) are genetically engineered recombinant protein sequences consisting of repeating units of silk-like and elastin-like blocks. By combining these entities, we show that both the characteristic strength of silk and the temperature-dependent responsiveness of elastin can be leveraged to create an enhanced stimuli-responsive material. We hypothesize that SELP behavior can be influenced by varying the silk-to-elastin ratio. If the responsiveness of the material at different ratios is significantly different, this would allow for the design of materials with specific temperature-based swelling and mechanical properties. This study demonstrates that SELP fiber properties can be controlled via a temperature transition dependent on the ratio of silk-to-elastin in the material. SELP fibers were experimentally wet spun from polymers with different ratios of silk-to-elastin and conditioned in either a below or above transition temperature (T_t) water bath prior to characterization. The fibers with higher elastin content showed more stimuli responsive behavior compared to the fibers with lower elastin content in the hot (57~60°C) versus cold (4~7°C) environment, both computationally and experimentally. This work builds a foundation for developing SELP materials with well-characterized mechanical properties and responsive features.

Graphical abstract

Silk–elastin-like protein polymers (SELPs) are genetically engineered recombinant proteins that incorporate elements of both physically strong silk and temperature-responsive elastin sequences to function as stimuli-responsive materials. Both simulation and experimental data showed an

*For correspondence. Tel.: +1-617-353-2374. Tax: +1-617-353-6766. jywong@bu.edu.
†These authors contributed equally to the current work

agreement that the thermal responsive behavior of SELP fibers can be controlled by adjusting the ratio of silk-to-elastin blocks.

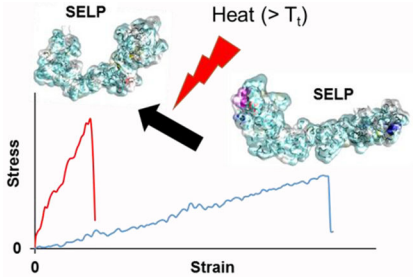

Keywords

Silk; elastin; computational modeling; wet-spinning; temperature responsive

1. Introduction

Stimuli-responsive systems are important in biomedical engineering because they allow for the triggered, controlled activation of an implanted or injected material [1–3]. For these systems, it is valuable to be able to predict the stimulated response and design new materials to have specific properties when triggered by a particular stimulus [4, 5]. As shown in Figure 1, this study focuses on one such stimuli-responsive biomaterial: fibers spun from silk-elastin-like-protein polymers (SELPs). SELPs seek to combine the advantageous properties of both strong, structurally-stable silk and temperature-responsive elastin. SELPs effectively have two triggered responses which generally scale with the elastin content: (1) swelling in water and (2) folding up of the molecular structure with increased temperature. The corresponding mechanisms are discussed in more detail below. While SELP biomaterials as protein monomer solutions, hydrogels, etc. have been explored in the literature [6–8], the triggered responses and the corresponding mechanisms that influence SELP fiber properties are not as well characterized.

In order to understand the behavior of SELPs, the individual entities that make up this block copolymer are first reviewed. Elastin is an extracellular matrix protein found in extensible tissues throughout the body where reversible recoil and resilience are essential [9–15]. Due to its responsive properties, elastin has been studied in the context of reversible switches that are based on temperature and other physical and chemical factors, such as pH, side chain identity, and ions [16–22]. In order to utilize this valuable material property for the design of responsive biomaterials in tissue engineering solutions, numerous studies have focused on elastin-like peptides and characterized the mechanisms behind this macroscopic tissue behavior [23–27]. *In vivo*, elastin assembly in the extracellular space occurs through coacervation or the association of monomers driven by interactions of hydrophobic domains; this is an endothermic, entropy-driven phase separation [28]. *In vitro*, elastin-like peptides have been shown to have an inverse temperature transition; elastin blocks are soluble in water below their transition temperature, but above this point, they undergo secondary

structure changes, self-assembling into an aggregate phase, which affects their material properties [9, 29–33].

Silks are fibrous proteins produced naturally by silkworms and spiders; they have Young's modulus values in the GPa range and have been used in their fibrous form for biomedical applications for centuries [34–36]. Recombinant silk can be used to incorporate these properties into hydrogel [37, 38], film [39], or fiber [40] biomaterials by using synthetic protein monomer solutions for fabrication; these recombinant silks can be chemically modified through their amino acid side chains [34, 41, 42]. This allows their properties to be altered or enhanced which is the method for the incorporation of elastin-like peptides into silk material sequences. The resulting combination of elastin and silk is a promising material for biomedical applications as SELPs are biocompatible, amenable to being spun into fibers, and possess stimuli-responsive tune-ability.

Designing this biomaterial requires fabricating the desired protein monomers, determining the necessary ratio of silk-to-elastin required for the material to exhibit properties of both of its component parts, and defining a range of temperatures and resulting mechanical properties that can be targeted to control tune-ability. For SELP fibers, the pertinent properties are the swelling behavior in water and the changes in mechanical properties below and above the transition temperature. Computational simulation is a helpful tool for initial predictions of material behavior. It can be used to understand how the molecular sequence and ratio of silk-to-elastin affect the resulting material, and it can serve as a guide for materials design when considering composition-property relationships [43].

In this study, we used simulation and experimental results for SELPs at different ratios of silk-to-elastin to learn how to predict material behavior. Three different ratios of silk to elastin were used throughout the simulation and experimental studies:

$$S1 = ((GVGVP)_4\,(GYGVP)(GVGVP)_3(GAGAGS))_{14}$$

$$S2 = ((GVGVP)_4\,(GYGVP)(GVGVP)_3(GAGAGS)(GAGAGS))_{12}, \text{ and}$$

$$S4 = ((GVGVP)_4\,(GYGVP)(GVGVP)_3(\mathit{GAGAGS})(\mathit{GAGAGS})(\mathit{GAGAGS})(\mathit{GAGAGS}))_9,$$

which have silk to elastin ratios of 1 to 8, 1 to 4, and 1 to 2 respectively. Briefly, in simulations, end-to-end length of the SE8Y sequence and the number of hydrogen bonds during molecular pulling for this sequence was characterized, demonstrating temperature responsive behavior. SASA (Solvent Accessible Surface Area) and radius of gyration were characterized for SE8Y and S4E8Y, showing more significant changes occurred for higher elastin content SELPs in response to changing temperature. Experimentally, synthesized SELPs were characterized for their purity and secondary structure prior to making fibers. SELPs with different elastin ratios (S2E8Y, S4E8Y) were wet spun, and their swelling behavior and mechanical properties were analyzed after conditioning in the different

temperature environments as outlined in Figure 2. This work presents the simulation predictions and the experimental material responses at low and high temperature conditioning in water for both materials; it seeks to relate molecular mechanisms seen in simulation to more macroscopic phenomena seen in experimental results and takes steps towards differentiating the behavior of SELP fibers as a function of their silk-to-elastin ratio. The methods and results presented here are meant to serve as a first step in establishing a data set of transition temperature and resulting mechanics for varying compositions of SELP fibers. Initial conclusions are drawn from work done at two temperatures and two ratios of silk to elastin; much additional work is required to be able to accurately predict behavior over a material and temperature range.

2. Results and Discussion

This work includes both simulation and experiments aimed at demonstrating trends in the elastin-concentration-dependent material behavior of SELP fibers. We will first detail the simulation results that provided the initial motivation to explore SELP fibers with tunable properties; these simulations help to explain the mechanisms for the behavior seen during experimentation. We will then detail the experimental results that support the simulation and demonstrate the tunable fiber behavior.

2.1. REMD (Replica Exchange Molecular Dynamics) Simulations

Models of single-molecule SE8Y were used to study temperature-dependent molecular mechanics using REMD simulation, as outlined in the experimental section. The rough transition temperature for the SE8Y sequence was originally determined experimentally (Section 2.3) to be in the range between 28-45°C using UV spectrophotometry – showing a significant change in optical density as temperature was increased across this range; the increase in optical density indicates a decrease in the size of the structure of the molecule [44]. Once the approximate transition temperature was known, the molecular structure was analyzed below (at 7°C) and above (at 57°C) this range using REMD simulations (Figure 3a). These simulations showed the end-to-end distance of the molecule decreased by 30% when measured at 57°C as compared to 7°C, consistent with a structural bend in the structure and the observed UV spectrophotometer result. Above the transition temperature, the structural collapse was similar to shorter elastin-like peptide contraction observed in earlier work [9]. This was supported by the experimental results in Section 2.3 that show increased temperature-triggered de-swelling in materials with greater elastin content.

The structural bend resulted in additional hydrogen bond formation, a contributing factor to mechanical strength, as demonstrated in the literature [45]. Molecular pulling simulations as in Tarakanova *et al.* were then conducted at high and low temperature, and intra-molecular hydrogen bonds were calculated as a function of the molecular displacement [44]. Throughout the deformation process, it was found that the high temperature structure retained approximately 15% more hydrogen bonds than the low temperature structure, suggesting increased stability above the transition-temperature (Figure 3b). The increased amount of hydrogen bonds suggested potential increased strength of fabricated materials. This was supported by the experimental results in Section 2.4 that show fibers with higher

elastin had greater increases in their moduli and ultimate tensile strengths above – when compared to below – their transition points.

2.2. Coarse-grained Simulations

The work done in REMD simulation provided insight into how silk-elastin materials behaved. However, in order to gauge how these properties were affected by the amount of elastin incorporated, coarse-grained simulations were used to compare two different ratios of silk-to-elastin. Atomistic models of SE8Y and S4E8Y, as predicted from REMD simulations, were coarse-grained using the PLUM potential and simulated at two temperatures of 7°C and 57°C. From Figure 4a and b, it is observed that CGMD (Coarse-Grained Molecular Dynamics) effectively captured the structural transition from low to high temperatures as these results agreed with both the experimental and REMD simulation data presented previously. Also, it can be noted that having a higher content of elastin-like sequence led to more significant changes in the dimension of the individual SELP molecule. The SASA (Solvent Accessible Surface Area) of SE8Y decreased by 8.6% while the radius of gyration was reduced by 22.8%. In contrast, for S4E8Y, the decrease in SASA was 1.9% and the radius of gyration decreased by 10.8%. The final protein conformations at both temperatures are illustrated in the insets of Figure 4c.

Furthermore, by plotting the amino acid contact maps in Figure 4c, variances in structural response to the different temperatures can be observed. An amino acid contact map served to visualize the distance matrix between all possible pairs of α-carbon atoms in every single amino acid in the SELP molecule. At low temperatures, SE8Y had a less compact structure where each amino acid was largely in contact with its nearest neighbors, as shown by the highly populated region near the diagonal of the matrix (Figure 4c, top left). Upon experiencing a structural transition at 57°C, it adopted a more compact structure, leading to greater numbers of contacts between amino acids that were much further away from each other, as seen by the increase in yellow regions away from the diagonal of the matrix (Figure 4c, top right). This corresponded to the significant reduction in the SASA and radius of gyration of the SE8Y molecule at 57°C (Figure 4a and b). In comparison, the S4E8Y molecule exhibited a compact structure at 7°C (inset of Figure 4c, bottom left) with significant numbers of contacts between amino acids that were more than a couple of hundreds of residues away, as highlighted by the significant amounts of yellow regions far away from the diagonal of the matrix (Figure 4c, bottom left). At 57°C, there was a reshuffling of the structure (inset of Figure 4c, bottom right), leading to decreased contacts with far neighbors in favor of nearer neighbors. This implied that the structure of the S4E8Y molecule was not able to become more compact. Moreover, it may have been favorable for the molecule to adopt a somewhat looser structure, leading to insignificant changes in its SASA and radius of gyration (Figure 4b) beyond the structural transition temperature, thus correlating with our experimental findings.

By considering the SASA, radius of gyration, and the contact maps, these results provided molecular insights into the differing changes in fiber diameters at the different temperatures observed in the experiments documented below. CGMD was not used to analyze hydrogen bonding, but data on the structural changes was hypothesized to be closely linked to the

relative numbers of hydrogen bonds. These simulations provided further mechanistic support for the experimental results detailed above and demonstrated there are ways to predict experimental results with simulation if solely the ratio of the elastin to silk content is known.

2.3. Synthesis of Polymers

SELPs were synthesized experimentally in order to explore and validate their temperature-responsive behavior. SELPs, named S2E8Y and S4E8Y as they have silk-to-elastin ratios of 2:8 and 4:8 respectively, were biosynthesized via seamless cloning strategies and purified via inverse temperature transition cycling as described previously (Figure 5a) [7]. The silk domain, containing the building block GAGAGS, was designed to provide β-sheet physical crosslinking for structural support of the wet-spun SELP fibers, while the elastin domain, GVGXP (X = V or Y), was encoded for thermal responsiveness. The purity of the synthesized proteins was confirmed by SDS-PAGE (Figure 5b). The molecular weight of each individual SELP construct was confirmed by MALDI-TOF. The measured molecular weights of S2E8Y and S4E8Y were 55 kDa and 48 kDa, respectively (Figure 4c and d), demonstrating that the materials were synthesized as intended.

The change in secondary structure of S2E8Y and S4E8Y during heating was monitored by circular dichroism (CD). Temperature-dependent CD spectra of S2E8Y during heating from 4 to 90°C showed that the silk content significantly affects the secondary structure of SELPs. Less ordered secondary structure is formed in SELP with higher elastin material, S2, than for the higher silk materials, S4, both below and above T_t (Figure 6a, c) [46]. The deconvolution spectra (Figure 6b, d) also suggested a significant increase (7%) for the ordered structures and a decrease in the unordered structures for S2E8Y during heating. These results demonstrated that the secondary structure of SELPs can be controlled by adjusting the ratio of silk-to-elastin blocks. While the protein properties determined by experimental measurements supported the simulation data and the ability to control temperature response with elastin to silk ratio, it was necessary to show that these properties also manifested in SELP fibers. Based on the characterization data above, temperature transition point was determined to be in the range of 28-45°C; therefore, conditioning temperatures were chosen that were well below (4°C) and above (60°C) this temperature range.

2.4. Fiber Diameter Measurement

The SELP properties simulated and studied experimentally were predicted to manifest themselves in the fabricated fibers in two ways: differences in fiber diameter change (swelling) and fiber tensile properties when S2E8Y and S4E8Y fibers were conditioned in water below and above the transition temperature. S2E8Y and S4E8Y fibers were successfully spun in a methanol coagulation bath and mounted onto frames in a water conditioning bath. We observed two swelling behaviors: swelling of fibers when they were transferred from methanol to water and de-swelling of these fibers in water once the temperature conditioning was applied. Change of fiber diameters from the methanol collection bath to the water conditioning bath are shown in Figure 7a. S2E8Y showed an immediate 2.3-fold increase in fiber diameter, while S4E8Y showed no change, indicating more swelling shown for the S2E8Y fibers. It is reported elsewhere that the elastin portion

of such composite materials will uptake water [47, 48]. Machado *et al.* reported on methanol-treated SELP fiber mats rapidly swelling and reaching maximum water uptake capacity within the first 2 minutes; they explained that the introduction of the elastin-like unit, which has a highly flexible conformation, increased the entire molecule's flexibility and water solubility by reducing the overall crystallinity of the system through the disruption of the silk-like blocks. This and other reports agree with our findings concerning the significant swelling behavior of S2E8Y, relatively higher elastin/silk ratio material, as compared to S4E8Y upon transfer from methanol to water as shown in Figure 7a.

Average diameters of fibers after conditioning in both temperature conditions are shown in Figure 7b. Percentages are of the diameter measured immediately after the fiber was placed in water prior to the start of incubation. Fiber diameter of S2E8Y was decreased to 64% after conditioning in the hot environment (oven, 60°C) and decreased to 80% after conditioning in the cold environment (refrigerator, 4°C). In contrast, S4E8Y showed no significant changes. This macroscopic observation is consistent with the molecular-level simulation results presented above. A similar observation was made in previous work showing the behavior of SELP or ELP materials [7, 49]. SELP hydrogel with higher elastin content shrunk more than the hydrogel with less elastin when the temperature was increased above the transition [7]. Carlson *et al.* reported gradual de-swelling and water loss behavior of ELP hydrogel with increasing temperature [49].

2.5. Fiber Mechanical Testing

In order to look at mechanical properties of fibers, all conditioned fibers were stretched on a custom-built uniaxial tensile tester (Figure 8a) [50]. From these tensile test results, maximum stresses, maximum strains, and the moduli of elasticity were calculated and compared. Several observations were made when observing differences between the two materials; these results agreed with the simulation predictions. Simulation data showed that 15% more hydrogen bonds were formed as the temperature increased, suggesting that SELP was more stabilized and potentially stronger above the transition temperature. Results from the mechanical tests of S2E8Y and S4E8Y confirmed these predictions for the SELP fiber. High temperatures increased the average tensile modulus of S2E8Y from 80 kPa to 508 kPa. S4E8Y also showed increased tensile modulus but to a lesser extent relative to S2E8Y, from 393 kPa to 589 kPa. In addition, it was shown that average failure stress was also increased from 182 kPa to 233 kPa for S2E8Y and from 472 kPa to 507 kPa for S4E8Y.

As expected for a material with a higher silk content, S4E8Y had a higher absolute average modulus in both the hot and cold conditions when compared to S2E8Y. However, while both materials showed a stiffening in the hot condition, the effect was enhanced with the increased amount of elastin as seen by the ratio of 6.4 between the hot and cold moduli for S2E8Y and a ratio of only 1.5 for S4E8Y as seen in Figure 8b. This is also visually evident in Figure 8a, which shows sample mechanical data for both materials at both conditions. This result agreed with the simulation data for hydrogen bonding as well as the simulated secondary structure analysis in Figure 5. The increased temperature resulted in increased ordered structure in S2E8Y as compared to S4E8Y, which was also apparent in the

mechanical testing as evident by the increased stiffening of the S2E8Y fiber as compared to the S4E8Y fiber.

Morphological characteristics can be seen in the two different materials via microscopy of fibers in water in Figure 7b as well as via SEM images in Figure 8c. S2E8Y fibers appeared to have smoother edges and more uniform internal structure as compared to the more textured S4E8Y. SEM images also showed a smooth surface for S2E8Y fibers and rougher surface for S4E8Y fibers. These results suggested that the silk blocks crystallized during shearing and formed aggregates during fiber formation.

3. Conclusions

In this study, we have demonstrated that SELP fibers have different de-swelling behavior and mechanical tensile strength below and above their transition temperatures; the change in these properties is enhanced as the elastin to silk ratio in the SELP polymer sequence increases. This behavior was originally analyzed using REMD and coarse-grained simulations at the molecular level where the exposed surface area and the radius of gyration significantly decreased for SE8Y (as compared to S4E8Y) above the transition temperature. This was supported at a macroscopic scale by showing the significantly decreased fiber diameters for S2E8Y (as compared to S4E8Y) conditioned in water above the transition temperature. Simulation also showed that during molecular pulling simulations below and above the transition temperature, the number of hydrogen bonds calculated above the transition temperature was greater than that below for SE8Y. This data suggested that there is potential for a difference in SELP fiber mechanical tensile strength above and below the temperature transition. This was supported by the stiffening of fibers conditioned in the hot condition; the increase in stiffness was greater for S2E8Y when compared to S4E8Y, further confirming that these dynamic properties scale with the elastin content. It is also important to note, however, that at too high of an elastin concentration, it becomes very difficult to fabricate fibers at all.

This work has made progress towards understanding how SELP fiber properties are affected by temperature. In order to leverage the temperature responsiveness of fibers, it is necessary to expand testing over a greater range of elastin to silk ratios such that for each sequence, a resulting modulus and de-swelling factor is known or can be predicted. It should also be determined how quickly the observed property changes occur once the material hits the transition temperature. Factors such as solution pH and fiber diameter should be evaluated for their effects on transition. By establishing a more robust understanding of the relationship between the elastin to silk ratio and the material properties, it will become easier to leverage these materials for biomedical applications. Triggered stiffening and/or de-swelling may allow for unique drug delivery methods, cell scaffolds, and wound healing applications in future experimentation.

4. Experimental Section

4.1. REMD Simulations

All REMD simulations and analysis were performed using methods previously reported [8]. In brief, the SELP sequence was constructed from the elastin domain (GXGVP) and silk domain (GAGAGS), where X indicates an interchangeable amino acid that plays a major role in the transition temperature of elastin. The GXGVP block represents the elastin, penta-peptide repeat unit that is used as a representative for elastin-like polymers [9]. The GAGAGS block represents silk as it adopts a structure similar to that of the *Bombyx mori* silkworm sequences. Two silk-elastin-like protein sequences were considered in simulation. SE8Y with eight elastin blocks and one silk block: $[(GVGVP)_4(GYGVP)(GVGVP)_3(GAGAGS)]_{14}$, and S4E8Y with eight elastin blocks and four silk blocks: $[(GVGVP)_4(GYGVP)(GVGVP)_3(GAGAGS)_4]_9$.

4.2. Coarse-grain Simulations

The equilibrated structure of both the SE8Y and S4E8Y molecules at 7°C was coarse-grained using the scheme as described in the PLUM potential [51], where the sidechains of each amino acid are combined into a single CG bead while the heavy atoms and their corresponding hydrogens in the protein backbone are fully represented. These beads are parameterized with implicit water solvent interactions. The mathematical formulation of the PLUM potential is laid out in the SI. The primary reason for applying CGMD to sample the SELPs' conformational changes is to significantly reduce the number of interactions and degrees of freedom in order to smoothen the rugged potential energy landscape encountered by atomistic MD. This greatly enhances the conformational sampling of the SELPs as the speedup factor is estimated to be faster by almost three orders of magnitude [52]. This speedup was determined by comparing the time to fold the protein having the sequence $(AAQAA)_3$ experimentally and with the PLUM potential. Experimental results showed that this protein folds in the order of 100 – 500 ns at room temperature while the same protein folding from an extended conformation with the PLUM potential was achieved within 500 ps of simulation time [52]. Such a significant acceleration in conformational sampling allows a drastic reduction in the amount of computational resources as compared to sampling with atomistic MD alone.

The PLUM potential is implemented in the open-source CGMD software package, Extensible Simulation Package for Research on Soft matter (ESPResSo) [53, 54]. The structural transition of both SE8Y and S4E8Y was determined at the temperatures of 7°C and 57°C with a simulation time of 5 ns each, corresponding to more than 1 μs of real sampling time based on a conservative estimate of the speedup factor [52]. The simulations were performed at constant volume with the temperature being controlled by a Langevin thermostat and a time step of 1 fs was used. Before each simulation, the non-bonded interactions are slowly uncapped over 1 ps. This minimizes any structural perturbations upon starting the simulation. GROMACS analysis tools [55], Visual Molecular Dynamics (VMD) [56, 57], in-house Bash and Python scripts, and script libraries such as MDTraj [58] were used to obtain each molecule's radius of gyration, solvent accessible surface area (SASA), and

contact maps. The values for the radius of gyration and SASA were averaged over the last 2.5 ns of the corresponding simulations.

4.3. Synthesis of Polymers

As shown in Figure 4a, the expression plasmid of SELPs, named S2E8Y and S4E8Y, were constructed using our previously established procedures and expressed under the T7 promoter in *E. coli* strain BL21Star (DE3) (Invitrogen, Carlsbad, CA, USA) in a New Brunswick BioFlo 3000 bioreactor (New Brunswick Scientific, Edison, NJ, USA) [59]. The protein was purified by the inverse transition cycling (ITC) method, as described previously [7]. The purity of the proteins was monitored via sodium dodecyl sulfate polyacrylamide gel electrophoresis (SDS-PAGE), and the molecular weight of SELPs were determined by matrix assisted laser desorption ionization-time of flight mass spectrometry (MALDI-TOF).

4.4. Fiber Spinning

In order to understand how fiber properties were affected by these molecular mechanisms and how the amount of elastin influenced the extremity of the changes, two materials with different silk/elastin ratio were considered experimentally, S2E8Y and S4E8Y. The material that was simulated, SE8Y, could not be processed into an actual fiber; this is most likely due to the relatively small amount of silk, which is the portion that affects the ability to spin into a fiber. Therefore, S2E8Y was chosen to be used as a comparison to S4E8Y for experimental characterization. Silk-elastin-like protein monomer (either S2E8Y or S4E8Y) was massed out into a 1.5 mL micro tube. Chilled DI water was added to make a 30 wt-% solution with gentle pipetting. The solution was transferred to a 250 μL Hamilton Gas Tight Syringe (1725 LTSN SYR, Hamilton Company, NV) with 32 gauge built in needle to generate high shear force. The syringe was mounted vertically on a syringe pump (Fusion 100, Chemyx Inc., TX) set to extrude at a flow rate of 5 μL/min approximately 10 cm above the bench top (Figure 2). The tip of the syringe was placed in a tall beaker full of a 100% methanol (Sigma-Aldrich, St. Louis, MO, USA) coagulation bath and fibers were formed as material exited the tip and fell to the bottom of the beaker. Fibers were left in the methanol undisturbed for at least 24 hours prior to manipulation. Transparent film (3M, Maplewood, MN) was used to fabricate frame holders to allow for easier manipulation of mounted SELP fibers during characterization as described in the Fiber Mounting section below.

4.5. Secondary Structure Characterization

Circular Dichroism (CD) spectra of 0.1 mg/mL SELP aqueous solutions were obtained on an Aviv model 62DS spectrophotometer equipped with a Peltier temperature controller (Aviv Biomedical, Lakewood, NJ). Quartz cuvettes with 1 mm path length were used. Temperature dependent CD scans were performed at 250 to 185 nm with a resolution of 0.5 nm at 4 to 90°C with 10 min equilibration at each temperature. The reversibility of the CD spectra was measured by scanning over a decreasing temperature range with the same equilibration period. The deconvolution of CD spectra was performed using DICHROWEB.

4.6. Fiber Morphology Characterization:

Scanning electron microscopy (SEM) was used to characterize fiber morphology. Samples were coated with gold and then observed using a Carl Zeiss (Carl Zeiss SMT, Germany) Ultra 55 field emission scanning electron microscope (FESEM) with an accelerated voltage of 5 kV.

4.7. Fiber Mounting and Diameter Measurement

Using forceps and scissors, approximately 2 cm long sample fibers were cut and mounted onto the transparent film frames [60, 61]. Double-sided tape was used to mount the fiber in place. Frame mounted fibers were easily manipulated for brightfield microscope imaging at 20x magnification without damage. Image J was used to calibrate the brightfield images and measure fiber diameter (by measuring width and ignoring curvature); the assumed diameter was the average of 5 measurements for each fiber image.

4.8. Fiber Temperature Conditioning and Mechanical Testing

S2E8Y and S4E8Y fibers mounted on frames were submerged in water in Petri dishes and conditioned at either the cold (4 °C, refrigerator) or hot (60 °C, oven) temperature for 48 hours [62]. After conditioning, additional tape was placed on top of the fiber mounted points to further secure them for mechanical testing. Microscope images were taken for each of the fibers to obtain diameters using an Axiovert S-100 microscope (Carl Zeiss AG, Oberkochen, Germany). The images were taken of the fibers while they were still in the coagulation bath solution methanol, when they were submerged and conditioned in water and also after the temperature conditioning step. Cross-sectional areas were calculated for stress calculations of mechanical characterization based on measured fiber diameters. A custom-built uniaxial tensile tester (capable of sensing mN forces) was used to stretch the fibers at a constant rate of elongation and measure the forces during stretching while keeping fibers in their conditioned water environments [50]. Once the frame was fixed on both sides of the holder, the frame was gently cut using scissors before performing stretching. The fiber was stretched at a rate of 5% of its initial length per second until the fiber broke (strain required varied with material and conditions). Max stress, max strain, modulus of elasticity, and toughness were measured by analyzing stress-strain data. These mechanical properties were compared between materials at both temperature conditions.

Acknowledgments

The authors thank NIH U01 EB014976-05 (M.J. Buehler, D.L. Kaplan, J.Y. Wong) for support of this work. N. Rim is a Howard Hughes Medical Institute International Student Research fellow. Computational simulations were performed on the Extreme Science and Engineering Discovery Environment (XSEDE), which is supported by the National Science Foundation grant number ACI-1053575, the MIT Engaging Cluster, and Singapore's A*STAR Computational Resource Centre and National Supercomputing Centre. J. Yeo acknowledge support from Singapore's Agency for Science, Technology and Research (A1786a0031). E. G. Roberts, N. Rim and W. Huang contributed equally on this work.

References

[1]. Chilkoti A, Dreher MR, Meyer DE, Raucher D, Advanced Drug Delivery Reviews 2002, 54, 613. [PubMed: 12204595]

[2]. Mart RJ, Osborne RD, Stevens MM, Ulijn RV, Soft Matter 2006, 2, 822.

[3]. Hu X, Zhang Y, Xie Z, Jing X, Bellotti A, Gu Z, Biomacromolecules 2017, 18, 649. [PubMed: 28212005]

[4]. Cross MC, Toomey RG, Gallant ND, Biomed Mater 2016, 11, 022002. [PubMed: 26942693]

[5]. Rim NG, Roberts EG, Ebrahimi D, Dinjaski N, Jacobsen MM, Martin-Moldes Z, Buehler MJ, Kaplan DL, Wong JY, Acs Biomaterials Science & Engineering 2017, 3, 1542. [PubMed: 28966980]

[6]. Huang W, Rollett A, Kaplan DL, Expert Opinion on Drug Delivery 2015, 12, 779. [PubMed: 25476201]

[7]. Huang WW, Tarakanova A, Dinjaski N, Wang Q, Xia XX, Chen Y, Wong JY, Buehler MJ, Kaplan DL, Adv Funct Mater 2016, 26, 4113. [PubMed: 28670244]

[8]. Tarakanova A, Huang W, Qin Z, Kaplan DL, Buehler MJ, ACS Biomaterials Science & Engineering 2017.

[9]. Tarakanova A, Huang W, Weiss AS, Kaplan DL, Buehler MJ, Biomaterials 2017, 127, 49. [PubMed: 28279921]

[10]. Urry DW, J Phys Chem B 1997, 101, 11007.

[11]. Urry DW, Parker TM, J Muscle Res Cell M 2002, 23, 543.

[12]. Debelle L, Tamburro AM, Int J Biochem Cell B 1999, 31, 261.

[13]. McDaniel JR, Radford DC, Chilkoti A, Biomacromolecules 2013, 14, 2866. [PubMed: 23808597]

[14]. Kurzbach D, Hassouneh W, McDaniel JR, Jaumann EA, Chilkoti A, Hinderberger D, J Am Chem Soc 2013, 135, 11299. [PubMed: 23822733]

[15]. Roberts S, Dzuricky M, Chilkoti A, FEBS Letters 2015, 589, 2477. [PubMed: 26325592]

[16]. Urry DW, Prog Biophys Mol Bio 1992, 57, 23. [PubMed: 1549698]

[17]. Urry DW, Angewandte Chemie-International Edition in English 1993, 32, 819.

[18]. Luan CH, Parker TM, Prasad KU, Urry DW, Biopolymers 1991, 31, 465. [PubMed: 1868163]

[19]. Reiersen H, Clarke AR, Rees AR, Journal of Molecular Biology 1998, 283, 255. [PubMed: 9761688]

[20]. Reiersen H, Rees AR, Biochemistry-Us 1999, 38, 14897.

[21]. Arkin H, Bilsel M, Aip Conf Proc 2009, 1203, 1211.

[22]. Arkin H, Bilsel M, Eur Phys J E 2010, 31, 327. [PubMed: 20229015]

[23]. Li B, Alonso DOV, Daggett V, J Mol Biol 2001, 305, 581. [PubMed: 11152614]

[24]. Rousseau R, Schreiner E, Kohlmeyer A, Marx D, Biophys J 2004, 86, 1393. [PubMed: 14990469]

[25]. Li B, Alonso DOV, Daggett V, Structure 2002, 10, 989. [PubMed: 12121654]

[26]. Ribeiro A, Arias FJ, Reguera J, Alonso M, Rodriguez-Cabello JC, Biophys J 2009, 97, 312. [PubMed: 19580769]

[27]. Martin L, Alonso M, Girotti A, Arias FJ, Rodriguez-Cabello JC, Biomacromolecules 2009, 10, 3015. [PubMed: 19795832]

[28]. Muiznieks LD, Keeley FW, Biochimica et Biophysica Acta (BBA) - Molecular Basis of Disease 2013, 1832, 10.

[29]. Urry DW, Long MM, Sugano H, J Biol Chem 1978, 253, 6301. [PubMed: 681352]

[30]. Cook WJ, Einspahr H, Trapane TL, Urry DW, Bugg CE, Journal of the American Chemical Society 1980, 102, 5502.

[31]. Cox BA, Starcher BC, Urry DW, Biochim Biophys Acta 1973, 317, 209. [PubMed: 4124839]

[32]. Urry DW, J Protein Chem 1988, 7, 1. [PubMed: 3076447]

[33]. Xia XX, Xu QB, Hu X, Qin GK, Kaplan DL, Biomacromolecules 2011, 12, 3844. [PubMed: 21955178]

[34]. Vepari C, & Kaplan DL , Progress in Polymer Science 2007, 32, 17.

[35]. Perez-Rigueiro J, Viney C, Llorca J, Elices M, J Appl Polym Sci 2000, 75, 1270.

[36]. Cunniff PM, Fossey SA, Auerbach MA, Song JW, Kaplan DL, Adams WW, Eby RK, Mahoney D, Vezie DL, Polymers for Advanced Technologies 1994, 5, 401.

[37]. Ayub ZH, Arai M, Hirabayashi K, Biosci Biotech Bioch 1993, 57, 1910.
[38]. Kapoor S, Kundu SC, Acta Biomaterialia 2016, 31, 17. [PubMed: 26602821]
[39]. Demura M, Asakura T, Journal of Membrane Science 1991, 59, 39.
[40]. Li GH, Liu H, Li TD, Wang JY, Mat Sci Eng C-Mater 2012, 32, 627.
[41]. Gotoh Y, Tsukada M, Minoura N, J Biomed Mater Res 1998, 39, 351. [PubMed: 9468042]
[42]. Johansson J, Rising A, Front Bioeng Biotechnol 2014, 2, 50. [PubMed: 25414847]
[43]. Ukpebor OT, Shah A, Bazov E, Boutis GS, Soft Matter 2014, 10, 773. [PubMed: 24511323]
[44]. Anna Tarakanova WH, Qin Zhao, Kaplan David L., and Buehler Markus J., ACS Biomaterials Science & Engineering, In Press.
[45]. Keten S, Buehler MJ, Nano Lett 2008, 8, 743. [PubMed: 18269263]
[46]. Greenfield NJ, Nat Protoc 2006, 1, 2876. [PubMed: 17406547]
[47]. Annabi N, Fathi A, Mithieux SM, Martens P, Weiss AS, Dehghani F, Biomaterials 2011, 32, 1517. [PubMed: 21115195]
[48]. Machado R, da Costa A, Sencadas V, Garcia-Arevalo C, Costa CM, Padrao J, Gomes A, Lanceros-Mendez S, Rodriguez-Cabello JC, Casal M, Biomed Mater 2013, 8, 065009. [PubMed: 24287397]
[49]. Trabbic-Carlson K, Setton LA, Chilkoti A, Biomacromolecules 2003, 4, 572. [PubMed: 12741772]
[50]. Backman DE, LeSavage BL, Wong JY, J Biomech 2017, 51, 118. [PubMed: 27923480]
[51]. Bereau T, Deserno M, The Journal of Chemical Physics 2009, 130, 235106. [PubMed: 19548767]
[52]. Bereau T, 2011.
[53]. Limbach HJ, Arnold A, Mann BA, Holm C, Computer Physics Communications 2006, 174, 704.
[54]. Arnold A, Lenz O, Kesselheim S, Weeber R, Fahrenberger F, Roehm D, Košovan P, Holm C, “ESPResSo 3.1: Molecular Dynamics Software for Coarse-Grained Models”, in Meshfree Methods for Partial Differential Equations VI, Griebel M and Schweitzer MA, Eds., Springer Berlin Heidelberg, 2013, p. 1.
[55]. Abraham MJ, Murtola T, Schulz R, Páll S, Smith JC, Hess B, Lindahl E, SoftwareX 2015, 1-2, 19.
[56]. Humphrey W, Dalke A, Schulten K, Journal of Molecular Graphics 1996, 14, 33. [PubMed: 8744570]
[57]. Schrödinger L, “The PyMOL Molecular Graphics System, Version 1.8 Schrödinger, LLC”, 2016.
[58]. McGibbon Robert T., Beauchamp Kyle A., Harrigan Matthew P., Klein C, Swails Jason M., Hernández Carlos X. Schwantes Christian R., Wang L-P, Lane Thomas J., Pande Vijay S., Biophysical Journal 2015, 109, 1528. [PubMed: 26488642]
[59]. Wang Q, Xia X, Huang W, Lin Y, Xu Q, Kaplan DL, Adv Funct Mater 2014, 24, 4303. [PubMed: 25505375]
[60]. Jacobsen MM, Li D, Gyune Rim N, Backman D, Smith ML, Wong JY, Sci Rep 2017, 7, 45653. [PubMed: 28378749]
[61]. Li D, Jacobsen MM, Gyune Rim N, Backman D, Kaplan DL, Wong JY, Biofabrication 2017, 9, 025025. [PubMed: 28471354]
[62]. Fernández-Colino A, Arias FJ, Alonso M, Rodríguez-Cabello JC, Biomacromolecules 2014, 15, 3781. [PubMed: 25230341]

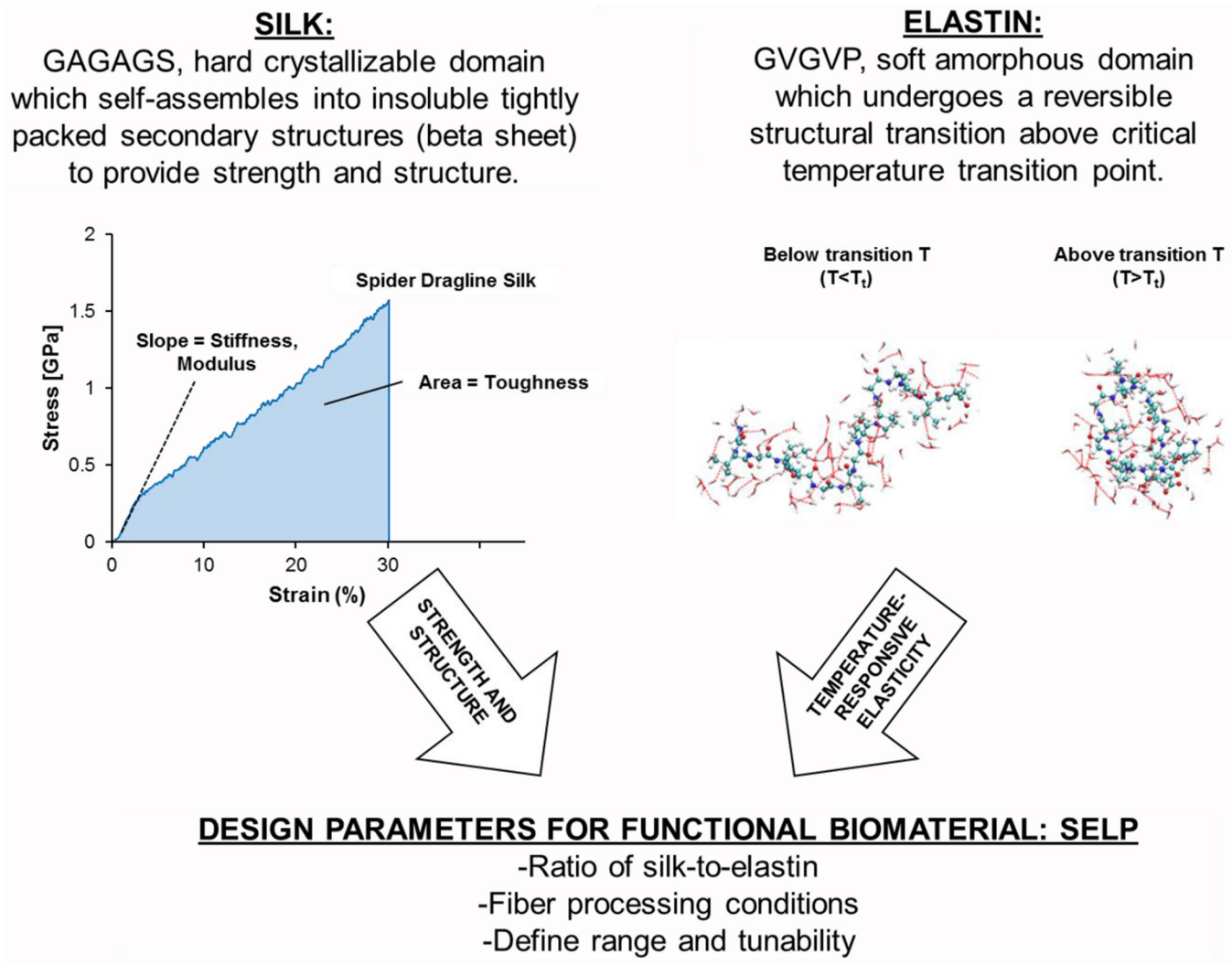

Figure 1.

Motivation for the study. The biomaterials studied in this paper, fibers spun from silk-elastin-like-protein polymers (SELPs), seek to combine the advantageous properties of both silk and elastin. Silk is spinnable and provides strength and structure to the fiber while elastin allows for a temperature-triggered, reversible change in molecular structure and corresponding fiber properties.

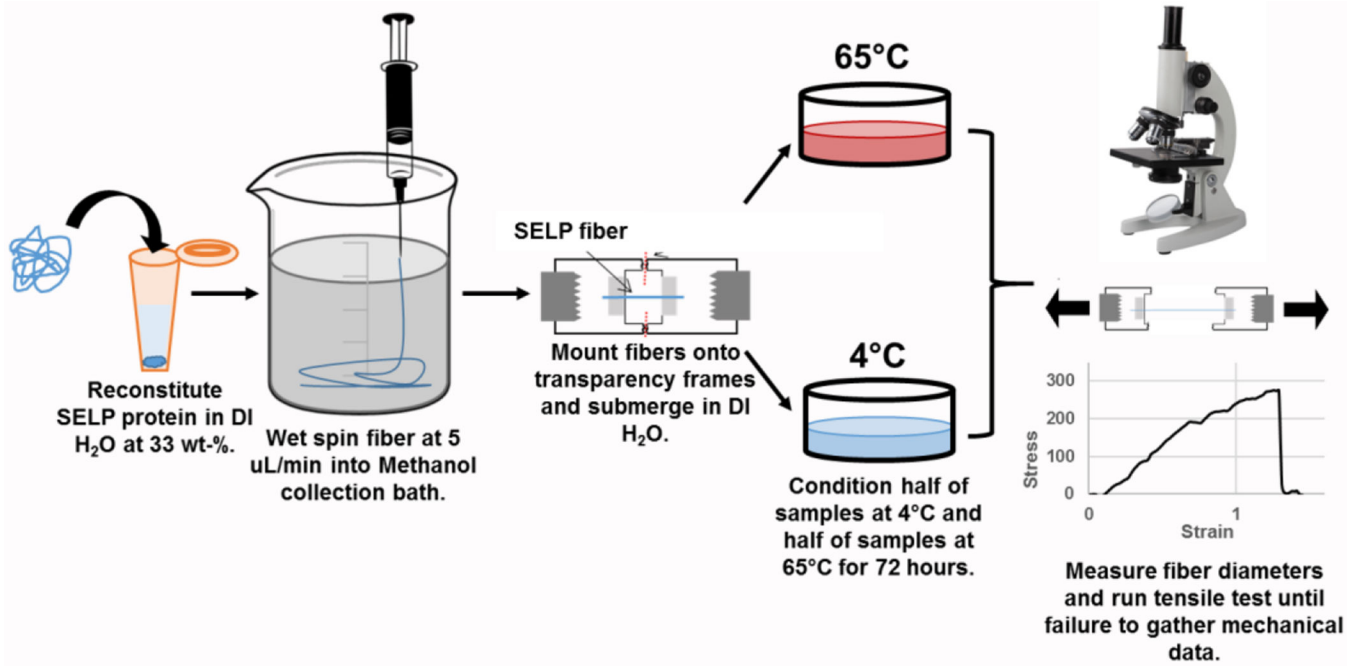

Figure 2.

Process overview for fiber spinning and their structural, functional characterization. In brief, SELPs were reconstituted in water, wet spun into a methanol bath, mounted onto frames for conditioning at the hot and cold conditions, and then analyzed using optical microscopy and a uniaxial tensile tester.

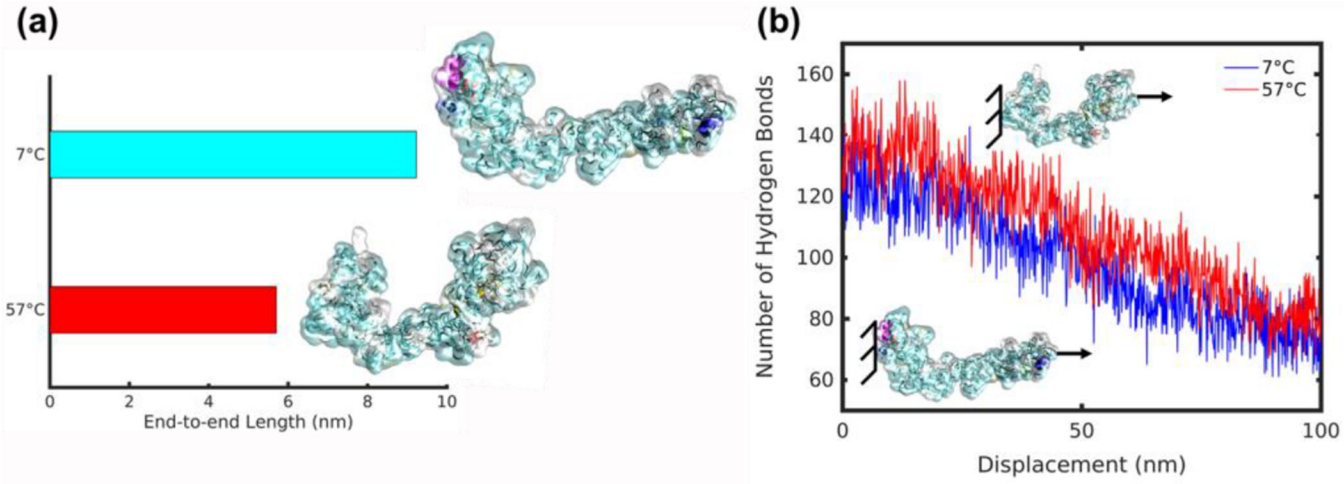

Figure 3.

Simulation data for silk–elastin-like protein polymers. (a) End-to-end length of the SE8Y sequence at 7°C and 57°C. Corresponding molecular structures are shown on the right. (b) Number of hydrogen bonds calculated during molecular pulling simulations at 7°C and 57°C. Molecular pulling setup shown for high temperature (top image) and low temperature (bottom image).

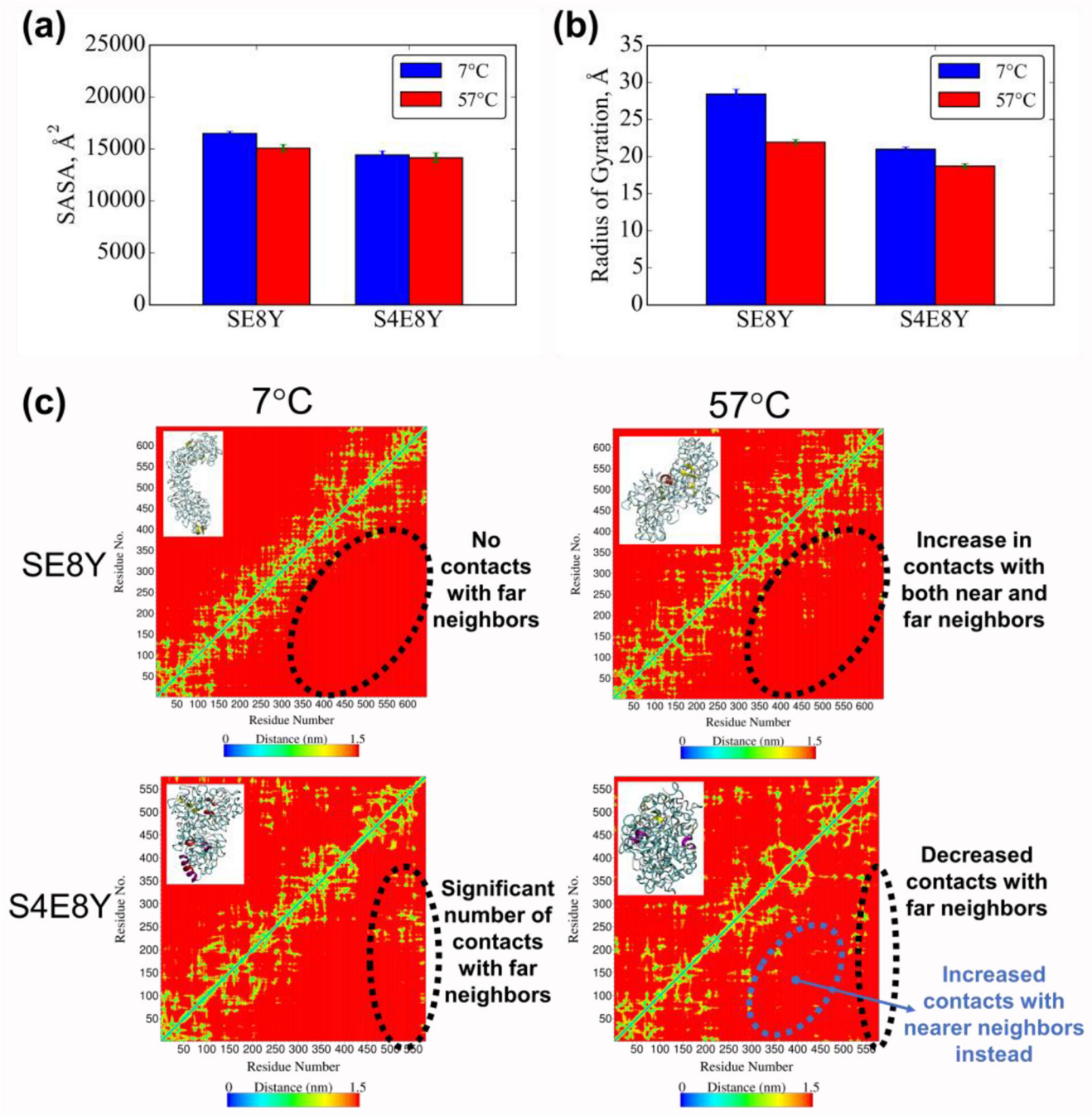

Figure 4.

Simulation data for SE8Y and S4E8Y at the two temperatures of 7°C and 57°C. (a) SASA and (b) radius of gyration respectively significantly decreased for SE8Y at 57°C, whereas S4E8Y only experienced minor decreases, relatively. (c) Variations in the contact maps for each protein with their corresponding conformations (insets).

(a)

SELP type	Sequence	
S	$(SE8Y)_{14}$	$((GVGVP)_4(GYGVP)(GVGVP)_3(GAGAGS))_{14}$
S2	$(S2E8Y)_{12}$	$((GVGVP)_4(GYGVP)(GVGVP)_3(GAGAGS)(GAGAGS))_{12}$
S4	$(S4E8Y)_9$	$((GVGVP)_4(GYGVP)(GVGVP)_3(GAGAGS)(GAGAGS)(GAGAGS)(GAGAGS))_9$

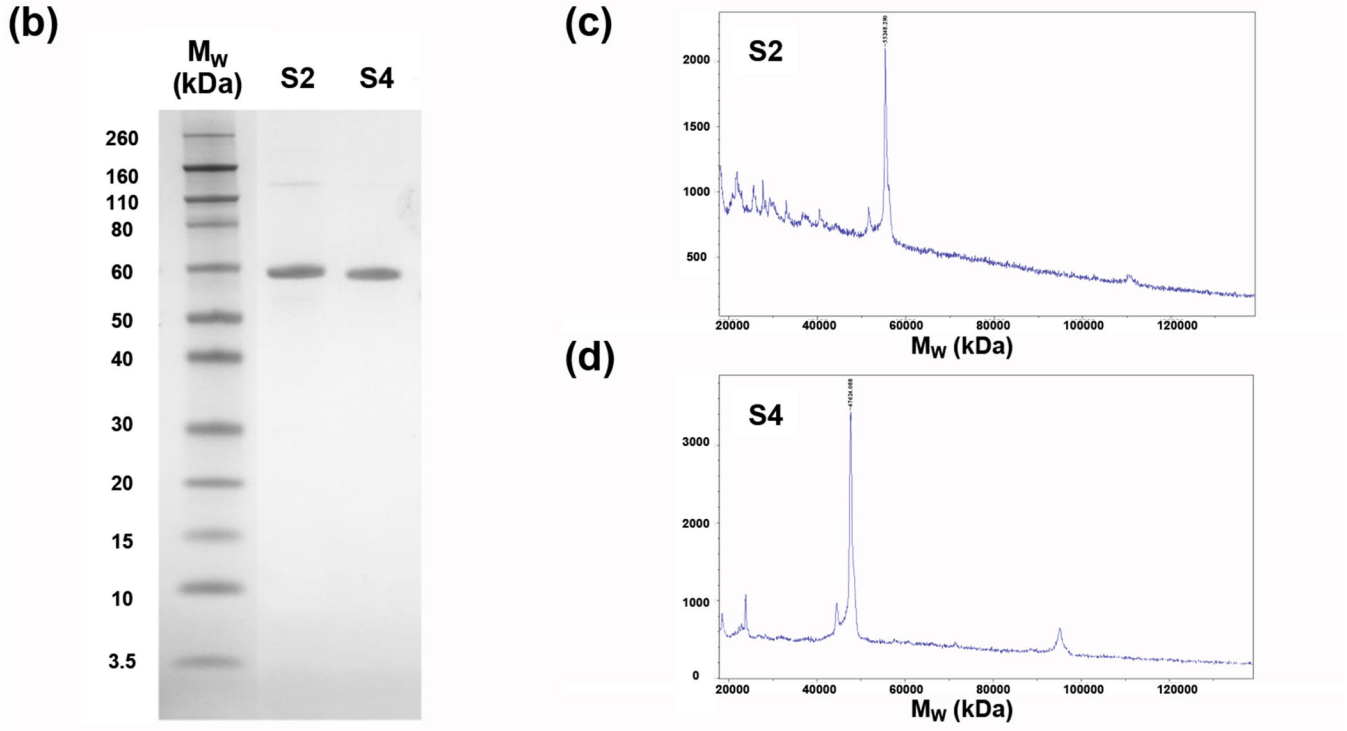

Figure 5.

Characterization of purified silk–elastin-like protein polymers (SELPs). (a) Constructs of silk–elastin-like proteins with different silk-to-elastin ratio. (b) Coomassie-stained 4–12% SDS-PAGE gel analysis of purified SELPs. The purity of target SELPs was confirmed by SDS-PAGE (lane 2: S2 and lane 3: S4). MALDI-TOF spectrum of SELPs confirming the molecular weight of (c) S2 and (d) S4. S2 indicates S2E8Y and S4 indicates S4E8Y.

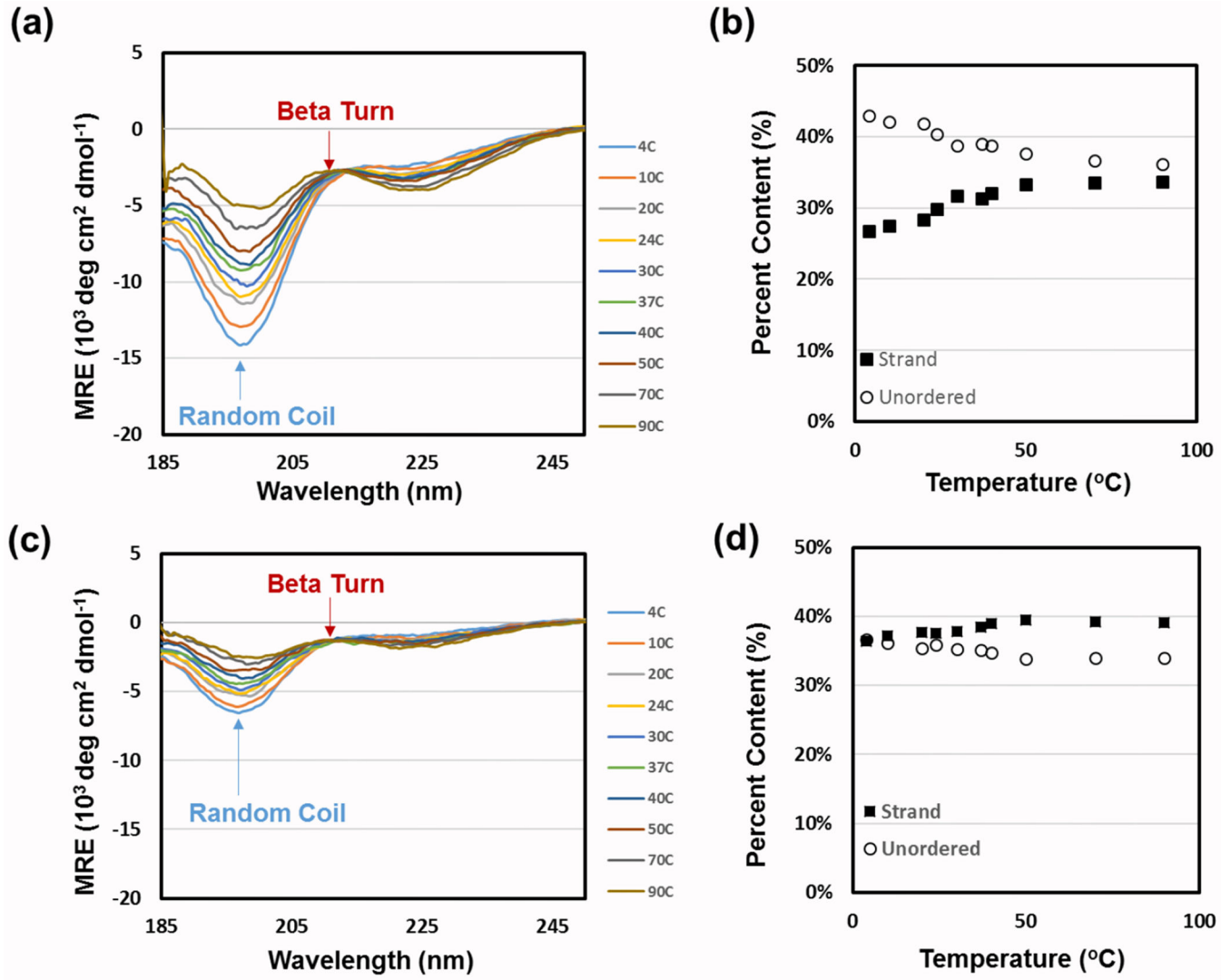

Figure 6.

Temperature-dependent CD spectra of S2 (a,b) and S4 (c,d) shows evidence that the silk content significantly affects the secondary structure of SELPs. Less ordered secondary structure is formed in SELP with higher elastin material, S2, than for the higher silk materials, S4, both below and above Tt. MRE: molar residue ellipticity. Unordered: structure that is neither sheet, helix, nor turn. S2 indicates S2E8Y and S4 indicates S4E8Y.

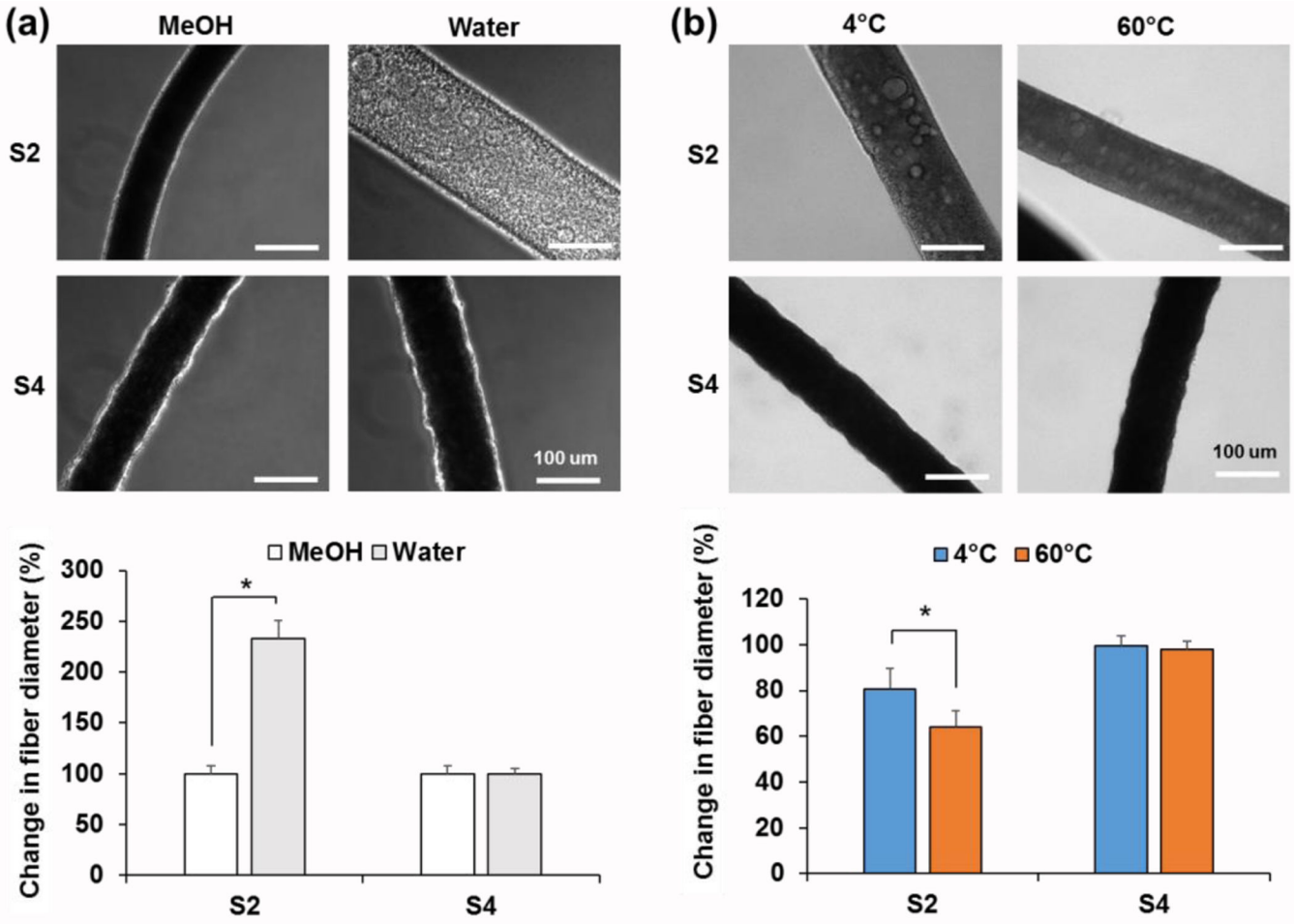

Figure 7.

Effect of water and temperature on fiber diameters. The fiber diameter change was analyzed by measuring diameter of the fiber from brightfield images. (a) The fiber's morphological change from methanol coagulation bath to water conditioning bath for future steps in procedure. The interaction with water caused the S2 fibers to swell significantly more than the S4 fibers. (b) The effect of temperature on SELP fibers. The fibers immersed in water were incubated in 60°C or 4°C for 48 hours prior to diameter measurements. High temperature showed significant structural change on S2 via diameter decreasing, while S4 did not show any significant change. S2 indicates S2E8Y and S4 indicates S4E8Y. (*, $p < 0.05$)

(a)

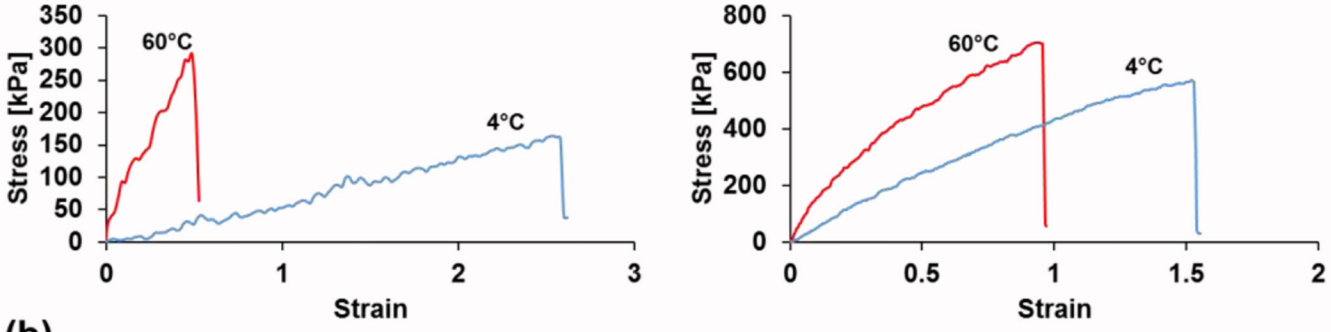

(b)

SELP type	Temperature	Modulus [kPa]	Modulus change (60°C/4°C)
S2	4°C	79.6±10.8	6.4±1.3
	60°C	508.0±107.0	
S4	4°C	393.1±17.1	1.5±0.5
	60°C	588.9±213.9	

(c)

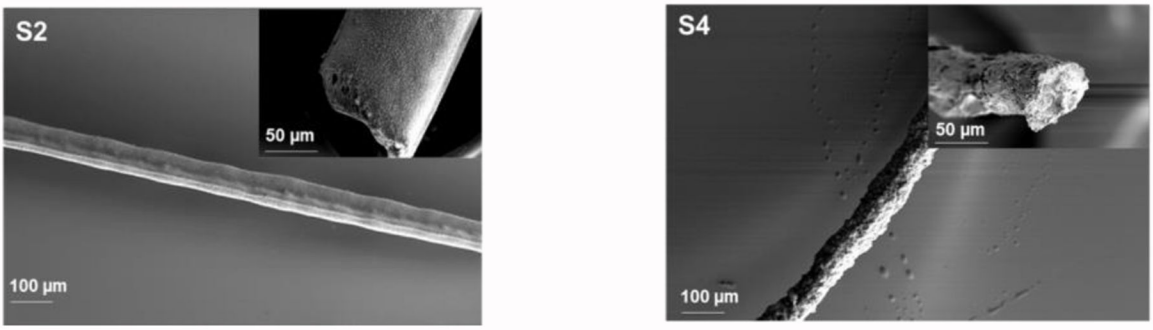

Figure 8.

(a) Mechanical characterization of the fibers conditioned in temperature controlled wet environment. (b) Stiffness (modulus) of S2 and S4 increased when fiber was conditioned in 60°C (>T_t) as compared to 4°C (<T_t). This transition is most likely due to the increased elastin content in S2 as a similar but much less dramatic change was seen for S4. (c) SEM images of S2 fiber and S4 fiber. The inlet images show higher magnification images of the same materials. S2 indicates S2E8Y and S4 indicates S4E8Y.